Duality structure of inclusive diffraction dissociation*

Keisho Hidaka
High Energy Physics Division, Argonne National Laboratory, Argonne, Illinois 60439
(Received 10 March 1977)

The duality structure of diffraction dissociation is studied in a triple-Regge (TR) analysis of the diffractive process $pp \to pX$. A scheme (normal scheme) is proposed which is quite different from the scheme previously suggested by many people (abnormal scheme). Diffractive resonance production is dual to the $P_tP_tP_0$ (Pomeron exchange) term in the abnormal scheme, whereas it is dual to the $P_tP_tR_0$ (ordinary Reggeon exchange) term in our normal scheme. From a careful TR analysis performed with much more data, we conclude that the data favor our normal scheme at least for $0.1 \lesssim |t| \lesssim 0.5$ $(\mathrm{GeV}/c)^2$. Here t is the mass squared of the external Pomeron (P_t).

I. INTRODUCTION

The duality structure of Reggeon-particle scattering can be studied by the analysis of inclusive cross sections, since an inclusive spectrum near the phase-space boundary is directly related to the absorptive amplitude of the Reggeon-particle forward scattering through Mueller's optical theorem. Here the question arises whether the usual Harari-Freund duality, which identifies the Pomeron exchange as the background term, works for Reggeon-particle scattering as well as for particle-particle scattering. Unlike the case of the meson Reggeon-particle scattering, where normal duality seems to work,[1] it is still uncertain whether normal duality holds for the case of Pomeron-particle scattering. According to Einhorn *et al.*[2] we expect an abnormal situation in which the cross section for diffractive resonances is described, on the average, by the triple-Pomeron term $P_tP_tP_0$, that is, resonances dual to Pomeron exchange. This scheme has been suggested phenomenologically by several authors.[3,4,5] In this paper, however, we propose a scheme (normal scheme) quite different from this current scheme. In our scheme the cross section for diffractive resonances is described, on the average, by the $P_tP_tR_0$ term, that is, resonances dual to meson Reggeon exchange. In previous papers[6,7,8] it has been shown that the data on the diffractive processes $pp \to pX$, $\pi^-p \to pX$, and $K^-p \to pX$ favor our normal scheme. In this article, by triple-Regge (TR) analysis of the high-energy inclusive data on $pp \to pX$ at Fermilab and at the CERN ISR,[9-15] we investigate in more detail (e.g., we perform the TR fit including interference terms) and with more care whether the experimental data favor the normal or abnormal duality scheme.

In the next section (Sec. II) we explain the duality schemes of diffraction dissociation. In Sec. III we test duality by a TR analysis assuming the absence of interference terms. In Sec. IV we check whether the inclusion of interference terms causes a drastic change in our conclusions obtained in Sec. III. In Sec. V we discuss the reliability of our duality test in comparison with the duality analysis of Field and Fox.[5] Section VI is devoted to conclusions.

II. DUALITY SCHEMES

We consider the process $p(p_1)+p(p_2) \to p(p_3)+$anything via the exchange of Pomeron and Reggeons in the t channel, as is depicted in Fig. 1(a). We define the invariants $s=-(p_1+p_2)^2$, $t=-(p_1-p_3)^2$, $M^2=-(p_1+p_2-p_3)^2$, and $\nu=M^2-m^2-t$, where m is the proton mass. In the limit of $M^2 \to \infty$ and $s/M^2 \to \infty$ one would expect, by analogy with particle-particle amplitudes, the Reggeon-particle amplitude ($ip \to jp$) to be described by the Regge-pole exchange of Fig. 1(b). This leads to the usual TR behavior for the inclusive cross section, i.e.,

$$\frac{s}{\pi}\frac{d\sigma}{dtd\nu}=\frac{\nu_0}{s}\sum_{ijk}G_{ijk}(t)\left(\frac{s}{\nu}\right)^{\alpha_i(t)+\alpha_j(t)}\left(\frac{\nu}{\nu_0}\right)^{\alpha_k(0)}. \quad (1)$$

The coupling G is the product $G_{ijk}(t)=\beta_i(t)\beta_j(t)\xi_i(t)\xi_j^*(t)\beta_k(0)g_{ijk}(t)/16\pi^2$, where β's are the usual Reggeon-particle-particle couplings, ξ's are the signature factors, $g_{ijk}(t)$ is the TR coupling, and ν_0 is taken as 1 $(\mathrm{GeV})^2$. Following the usual method[16] we can write the first-moment finite-mass sum rule (FMSR) for large $s/\bar{\nu}$ in the form

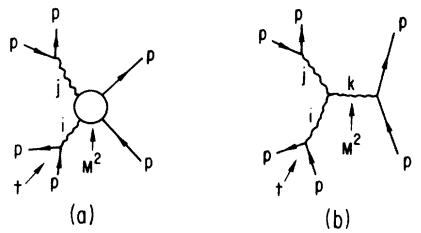

FIG. 1. (a) Reggeon-particle amplitude $ip \to jp$ and (b) TR diagram.

$$I \equiv \int_0^{\bar{\nu}} d\nu \frac{\nu}{\pi} \frac{d\sigma}{dtd\nu} = \frac{\nu_0}{s^2} \sum_{ijk} G_{ijk}(t)\, s^{\alpha_i(t)+\alpha_j(t)} \frac{\bar{\nu}^{\alpha_k(0)-\alpha_i(t)-\alpha_j(t)+2}}{\alpha_k(0)-\alpha_i(t)-\alpha_j(t)+2} \left(\frac{1}{\nu_0}\right)^{\alpha_k(0)} \equiv \sum_{ijk} G(ijk)\,. \tag{2}$$

Now we consider two-component duality for the absorptive forward amplitude of Reggeon-particle scattering ($ip \to jp$). Various arrangements (twists) of dual diagrams lead to various duality schemes (Appendix). There are three typical schemes. One is the normal scheme proposed by us. The second is the original abnormal scheme of Einhorn *et al.*[2] The third is the extreme abnormal scheme of Field and Fox (FF).[5] We propose a normal scheme

$$I(\text{background}) = \sum_{ij} G(ijP)\,, \tag{3}$$

$$I(\text{res}) = \sum_{ij} G(ijR)\,. \tag{4}$$

In the original abnormal scheme of Einhorn *et al.*, we have

$$I(\text{background}) = G(RRP)\,, \tag{5}$$

$$I(\text{res}) = G(PPP) + G(PPX) + G(\{PR\}R) + G(RRR) \tag{6}$$

with vanishing or very small PPR, PRP, and RPP terms for which there are no natural places in their duality rules. Stimulated by the suggestion of Einhorn *et al.*, FF proposed phenomenologically an extremely abnormal scheme,[17] that is,

$$I(\text{background}) = G(PPR) + G(\{PR\}P) + G(RRP)\,, \tag{7}$$

$$I(\text{res}) = G(PPP) + G(\{PR\}R) + G(RRR)\,. \tag{8}$$

Here $G(\{PR\}k) \equiv G(PRk) + G(RPk)$, and I(background) and I(res) are the background and resonance (including proton) integrals of the left-hand side (lhs) of Eq. (2), respectively. P is the Pomeron, R means the meson trajectories, and X, which was introduced by Einhorn *et al.*, represents lower-lying singularities (such as Reggeon-Reggeon cuts) with intercept $\alpha_X(0) \geq 0$ (presumably ≈ 0).[2] The term $G(PPP)$ in Eqs. (6) and (8) is called the abnormal dual component, that is, the PPP term dual to the diffractive resonances. In the following we investigate which scheme the experimental data favor.

III. DUALITY TEST WITHOUT INTERFERENCE TERMS[6]

There are very many high-energy and high-mass data on $pp \to pX$, so we can estimate the couplings $G_{ijk}(t)$ with good accuracy by fitting the data to the form of Eq. (1). In particular, these data cover so large a range of energy s, especially in the region $0.1 \lesssim |t| \lesssim 0.5$ (GeV/c),[2] that we can separate k = Pomeron (scaling) from k = meson Reggeon (nonscaling) contributions to the cross section with little ambiguity in this t region.[18] This separation is crucial for the duality argument. We can estimate the right-hand side (rhs) of Eqs. (3)–(8) using the TR parameters obtained this way. On the other hand, we can calculate the lhs of Eqs. (3)–(8) using the background-resonance-separated low-mass spectra in $0.1 \lesssim |t| \lesssim 0.5$ (GeV/c)^2.[19,20] In this way we can check which scheme such data dominated by the diffraction components favor

A. TR fit

1. Fitting procedure

We use only the TR formula Eq. (1) in the practical calculation of TR parameters without using the FMSR Eq. (2). Hence we input only high-s, *high-M^2* data[9-15] (see Table I, which also lists other data, not used[19-23]). We make four-term fits: PPP, RRP, PPR, and RRR in the normal and the extreme abnormal cases, and PPP, RRP, $\{PR\}R$, and RRR (abnormal I) or PPP, RRP, $\{PR\}R$, and PPX (abnormal II) in the original abnormal case. For the Regge trajectories in the "t" channel of $ip \to jp$ scattering, we keep the intercepts as $\alpha_P(0) = 1$, $\alpha_R(0) = \frac{1}{2}$, and $\alpha_X(0) = 0$.

Fitting formulas are as follows:

$$\frac{s}{\pi}\frac{d\sigma}{dtd\nu} = G_{PPP}(t)(1-x)^{1-2\alpha_P(t)} + G_{RRP}(t)(1-x)^{1-2\alpha_R(t)} + G_{PPR}(t)(1-x)^{1/2-2\alpha_P(t)}\left(\frac{\nu_0}{s}\right)^{1/2} + G_{RRR}(t)(1-x)^{1/2-2\alpha_R(t)}\left(\frac{\nu_0}{s}\right)^{1/2} \tag{9}$$

in the normal and the extreme abnormal cases,

$$\frac{s}{\pi}\frac{d\sigma}{dtd\nu} = G_{PPP}(t)(1-x)^{1-2\alpha_P(t)} + G_{RRP}(t)(1-x)^{1-2\alpha_R(t)} + G_{\{PR\}R}(t)(1-x)^{1/2-\alpha_P(t)-\alpha_R(t)}\left(\frac{\nu_0}{s}\right)^{1/2} + G_{RRR}(t)(1-x)^{1/2-2\alpha_R(t)}\left(\frac{\nu_0}{s}\right)^{1/2} \tag{10}$$

TABLE I. $pp \to pX$ cross-section data.

(a) High-M^2 data

s (GeV^2)	M^2 (GeV^2) or x	$-t$ or $p_\perp{}^2$ [(GeV/c)^2] or $p_\perp$ (GeV/c)	Reference
108, 213, 285, 503, 752	Plotted vs x $0.8 \lesssim x \lesssim 0.93$ (We use all)	$-t = 0.16, 0.20, 0.25$ 0.33	9 (Fermilab)
551	Plotted vs M^2 $0 \lesssim M^2 \lesssim 50$ (We only use $M^2 \gtrsim 17$)	$-t = 0.15, 0.35, 0.55,$ 0.65, 0.95, 1.25	10 (CERN)
930	Plotted vs M^2 $0 \lesssim M^2 \lesssim 140$ (We only use $M^2 \gtrsim 28$)	$-t = 0.35, 0.45, 0.55,$ 0.65, 0.75, 0.85, 0.95, 1.05, 1.15, 1.25, 1.35, 1.45, 1.55, 1.65, 1.75, 1.85, 1.95, 2.05, 2.25, 2.35	10 (CERN)
930	Plotted vs M^2 $0 \lesssim M^2 \lesssim 52$ (We only use $M^2 \gtrsim 28$)	$-t = 0.25, 0.35, 0.55,$ 1.05, 1.75	11 (CERN)
387	$M^2 \leq 5$ $5 \leq M^2 \leq 25$ $25 \leq M^2 \leq 50$ $50 \leq M^2 \leq 100$ (We only use $M^2 \gtrsim 15$)	Plotted vs t $0.0 \leq -t \leq 0.4$	12 (Fermilab)
387	Plotted vs x $0.5 \lesssim x \lesssim 1.0$ (We only use $0.8 \lesssim x \lesssim 0.96$, i.e., $15 \lesssim M^2 \lesssim 77$)	$-t = 0.05, 0.15,$ 0.25, 0.35	13 (Fermilab)
194, 763 (We only use $s = 194$)	Plotted vs x $0.6 < x < 1.0$ (We only use $0.80 \lesssim x \lesssim 0.97$, i.e., $6 \lesssim M^2 \lesssim 40$)	$p_\perp{}^2 = 0.05, 0.15, 0.30,$ 0.50 ($t \approx -p_\perp{}^2/x$)	14 (Fermilab)
100,360	Plotted vs x $0.78 \leq x \leq 0.94$ (We only use $0.8 \leq x$)	$-t = 0.33, 0.45$	15 (Fermilab)
566 (We do not use)	Plotted vs M^2 $0 \lesssim M^2 \lesssim 50$	$-t = 0.056, 0.094$	21 (Fermilab)
	$8 \lesssim M^2 \lesssim 14$ $20 \lesssim M^2 \lesssim 60$	Plotted vs t $0.019 < -t < 0.19$	
1995 (We do not use)	Plotted vs $0.3 \lesssim x \lesssim 1.0$	$p_\perp = 0.7, 0.8, 0.9,$ 1.0, 1.1, 1.2	22 (CERN)

(b) Low-M^2 data (not used in our TR fits)

s (GeV^2)	M (GeV)	$-t$ [(GeV/c)^2]	Reference
20.4	Plotted vs M $M \lesssim 2.0$	0.023, 0.044, 0.059, 0.12, 0.20, 0.29, 0.86, 0.88	20 (BNL)
30.2, 39.6, 57.6	Plotted vs M $M \lesssim 2.0$	0.044, 0.88	
46.9	Plotted vs M $M \lesssim 2.5$	$0.05 \lesssim -t \lesssim 6.0$	19, 23 (CERN)

in the abnormal-I case, and

$$\frac{s}{\pi}\frac{d\sigma}{dtd\nu}=G_{PPP}(t)(1-x)^{1-2\alpha_P(t)}+G_{RRP}(t)(1-x)^{1-2\alpha_R(t)}$$
$$+G_{\{PR\}R}(t)(1-x)^{1/2-\alpha_P(t)-\alpha_R(t)}\left(\frac{\nu_0}{s}\right)^{1/2}+G_{PPX}(t)(1-x)^{-2\alpha_P(t)}\frac{\nu_0}{s} \quad (11)$$

in the abnormal-II case. Here $x=1-\nu/s$ is Feynman's scale parameter. Fits to the data are performed at each fixed value of t [$t=-0.2$, -0.3, and -0.4 (GeV/c)^2], and the values of t-channel trajectories $\alpha_P(t)$ and $\alpha_R(t)$ are allowed to vary for an optimum fit. With this variation of $\alpha_R(t)$ we can effectively take π exchange into account.[24]

2. Data input

In the TR fits we use only the high-s, *high-M^2* data with $0.8 \leq x$ of Refs. 9–15 (Table I). The cross-section data at each value of t [$t=-0.2$, -0.3, and -0.4 (GeV/c)^2] are obtained by *interpolation* from the data near the t point with a simple exponential form.

3. Results of fits

Table II shows the TR parameters obtained this way.[25] Also shown are the optimum values of $\alpha_P(t)$ and $\alpha_R(t)$ in terms of $\alpha'_P(0)$ and $\alpha_R(0)$ with $\alpha_P(t)=1+\alpha'_P(0)t$ and $\alpha_R(t)=\alpha_R(0)+t$. Figure 2 shows how well these TR parameters reproduce the data.

4. Comparison with other TR analyses

Here we compare our TR fit with other TR analyses. There are two TR analyses that use the Fermilab and ISR data, that of Roy and Roberts (RR)[24] and that of Field and Fox (FF).[5] We summarize the outline of these analyses.

(I) TR analysis of RR[24]:

TABLE II. Estimations of TR parameters in Eqs. (9)–(11) by χ^2 fit.

Normal and extreme		Abnormal I		Abnormal II	
(a) Estimation at $t=-0.2$ (GeV/c)^2					
$\alpha'_P(0)$ [(GeV/c)$^{-2}$]	0.25	$\alpha'_P(0)$	0.05	$\alpha'_P(0)$	0.35
$\alpha_R(0)$	0.1	$\alpha_R(0)$	0.1	$\alpha_R(0)$	0.1
G_{PPP} (mb/GeV^2)	0.422 ± 0.069	G_{PPP}	0.349 ± 0.054	G_{PPP}	0.566 ± 0.036
G_{RRP}	40.2 ± 6.0	G_{RRP}	41.5 ± 5.9	G_{RRP}	37.1 ± 3.7
G_{PPR}	0.970 ± 0.350	$G_{\{PR\}R}$	16.9 ± 6.3	G_{PPX}	1.76 ± 0.99
G_{RRR}	7.35 ± 33.6	G_{RRR}	−77.2 ± 64.4	$G_{\{PR\}R}$	4.05 ± 4.15
χ^2	27.2	χ^2	27.9	χ^2	27.4
Degrees of freedom	90	Degrees of freedom	90	Degrees of freedom	90
(b) Estimation at $t=-0.3$ (GeV/c)^2					
$\alpha'_P(0)$ [(GeV/c)$^{-2}$]	0.35	$\alpha'_P(0)$	0.05	$\alpha'_P(0)$	0.15
$\alpha_R(0)$	0.1	$\alpha_R(0)$	0.1	$\alpha_R(0)$	0.1
G_{PPP} (mb/GeV^2)	0.334 ± 0.044	G_{PPP}	0.218 ± 0.020	G_{PPP}	0.266 ± 0.015
G_{RRP}	25.1 ± 4.3	G_{RRP}	26.6 ± 3.7	G_{RRP}	26.3 ± 2.8
G_{PPR}	0.715 ± 0.236	$G_{\{PR\}R}$	10.5 ± 3.4	G_{PPX}	0.489 ± 0.459
G_{RRR}	34.3 ± 26.9	G_{RRR}	−17.5 ± 43.0	$G_{\{PR\}R}$	7.31 ± 2.54
χ^2	34.9	χ^2	37.6	χ^2	36.8
Degrees of freedom	92	Degrees of freedom	92	Degrees of freedom	92
(c) Estimation at $t=-0.4$ (GeV/c)^2					
$\alpha'_P(0)$ [(GeV/c)$^{-2}$]	0.25	$\alpha'_P(0)$	0.05	$\alpha'_P(0)$	0.25
$\alpha_R(0)$	0.1	$\alpha_R(0)$	0.1	$\alpha_R(0)$	0.1
G_{PPP} (mb/GeV^2)	0.205 ± 0.024	G_{PPP}	0.138 ± 0.012	G_{PPP}	0.229 ± 0.012
G_{RRP}	22.2 ± 3.6	G_{RRP}	24.0 ± 3.2	G_{RRP}	22.1 ± 2.39
G_{PPR}	0.317 ± 0.123	$G_{\{PR\}R}$	6.61 ± 2.34	G_{PPX}	0.518 ± 0.324
G_{RRR}	18.07 ± 21.82	G_{RRR}	−25.8 ± 35.1	$G_{\{PR\}R}$	2.72 ± 2.02
χ^2	26.5	χ^2	27.9	χ^2	27.0
Degrees of freedom	86	Degrees of freedom	86	Degrees of freedom	86

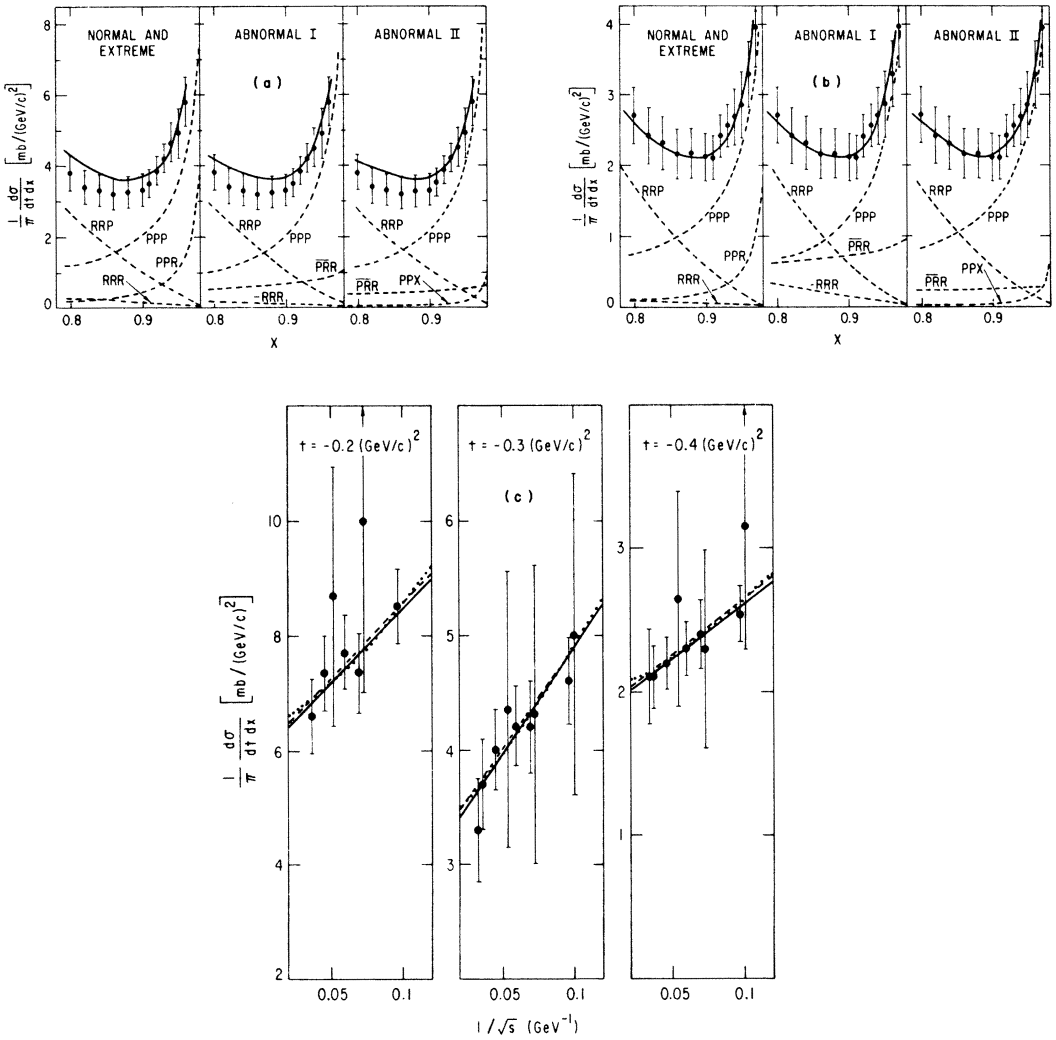

FIG. 2. (a) and (b) $pp \to pX$ cross-section data plotted against x at $s = 930$ GeV^2 and $t = -0.3$ (a) and -0.4 (b) (GeV/c)^2 (Refs. 10,11). The solid lines are the fitted curves of normal and extreme case fit, abnormal-I case fit, and abnormal-II case fit. (c) $pp \to pX$ cross-section data plotted against $1/\sqrt{s}$ at $x = 0.9$ and $t = -0.2$, -0.3, and -0.4 (GeV/c)^2. Solid, dashed, and dotted lines are the fitted curves of normal and extreme case fit, abnormal-I case fit, and abnormal-II case fit, respectively.

(1) Both TR formula Eq. (1) and FMSR Eq. (2) are used.

(2) Hence they input both high-M^2 (Refs. 9–12, 15, 22) and low-M^2 (Refs. 19, 20, 23) data.

(3) Four-term fit: PPP, RRP, PPR, and RRR without interference terms.

(4) $G_{ijk}(t)$ are fitted at each fixed t.

(5) The t-channel trajectories $\alpha_P(t)$ and $\alpha_R(t)$ are allowed to vary for the optimum fit. In $0 \lesssim -t \lesssim 0.8$ (GeV/c)^2 the results are described nearly by $\alpha_P(t) = 1.0 + 0.25t$ and $\alpha_R(t) = 0.2 + 0.5t$. As for the "t"-channel trajectories of $ip \to jp$ scattering, the intercepts are fixed as $\alpha_P(0) = 1$ and $\alpha_R(0) = \frac{1}{2}$.

(6) With this variation of $\alpha_R(t)$ π exchange is effectively taken into account.

(II) TR analysis of FF[5]:

(1) The same as (1) of RR.

(2) The same as (2) of RR [here the input data are from Refs. 9–12, 14, 21, 26 (high M^2) and Refs. 19, 20 (low M^2)].

(3) Six-term fit: PPP, PPR, RRP, RRR, $\pi\pi P$, and $\pi\pi R$ without interference terms.

(4) $G_{ijk}(t)$ are fitted by parametrizing in the exponential form.

(5) The Pomeron slope $\alpha'_P(0)$ with $\alpha_P(t) = \alpha'_P(0)\, t + 1$ is allowed to vary for an optimum fit; $\alpha'_P(0) = 0.36$ (solution 1) and $\alpha'_P(0) = 0.37$ (solution 2) are obtained, where solution 1 and solution 2 corre-

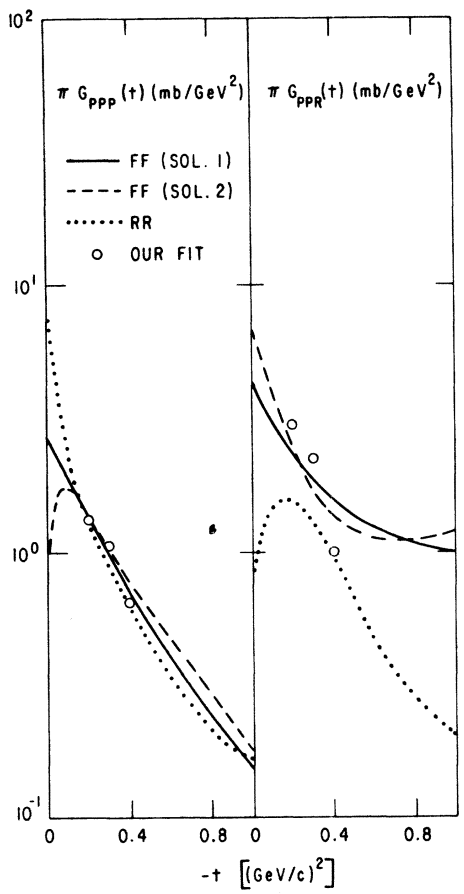

FIG. 3. TR couplings $G_{PPP}(t)$ and $G_{PPR}(t)$ in the TR analyses of RR (Ref. 24), FF (Ref. 5), and us (normal and extreme case fit). Here the normalization of $G_{ijk}(t)$ is determined by the TR formula (1).

spond to the parametrization with $G_{PPP}(0)\neq 0$ and $G_{PPP}(0)=0$, respectively. For the second leading trajectory, $\alpha_R(t)=t+\frac{1}{2}$ is taken. For the "t"-channel trajectories of $ip\to jp$ scattering, the intercepts are fixed as $\alpha_P(0)=1$ and $\alpha_R(0)=\frac{1}{2}$.

(6) The t-channel π exchange terms $\pi\pi P$ and $\pi\pi R$ are given by the theoretical estimation of Bishari.[24]

(III) Our TR fit (normal and extremely abnormal cases):

(1) Only TR formula Eq. (1) is used

(2) Hence only *high*-M^2 data are input[9-15] (Table I).

(3)–(6) The same as (3)–(6) of RR [optimum-fit values of the t-channel trajectories $\alpha_P(t)$ and $\alpha_R(t)$ are given in Table II].

The results of these three TR analyses are compared in Fig. 3. The agreement of the three is very good in $0.1\lesssim|t|\lesssim 0.5$ (GeV/c)^2 (we refer to this region as the T_1 region) while the disagreement between RR and FF is extremely large (almost order-1 difference) in $|t|\lesssim 0.1$ and $|t|\gtrsim 0.5$ (GeV/c)^2 (we refer to this region as the T_2 region) especially in the relative size of G_{PPP} and G_{PPR}.

We can explain the reason of this large disagreement as follows. In Fig. 4 the data points are plotted in an s-t plane. As is seen from Fig. 4 and Table I the data in the T_2 region have very small density and *cover a very narrow s range*. The TR couplings are fitted in the parametrization of $G_{ijk}(t)=a_1e^{b_1t}+a_2e^{b_2t}$ in the FF case. Noting the small data density in the T_2 region and the very large data density in the T_1 region, we can say that these parameters a_1, b_1, a_2, and b_2 (especially the relative size of G_{ijP} and G_{ijR})[27] are mainly determined by the T_1-region data. So the FF estimations of

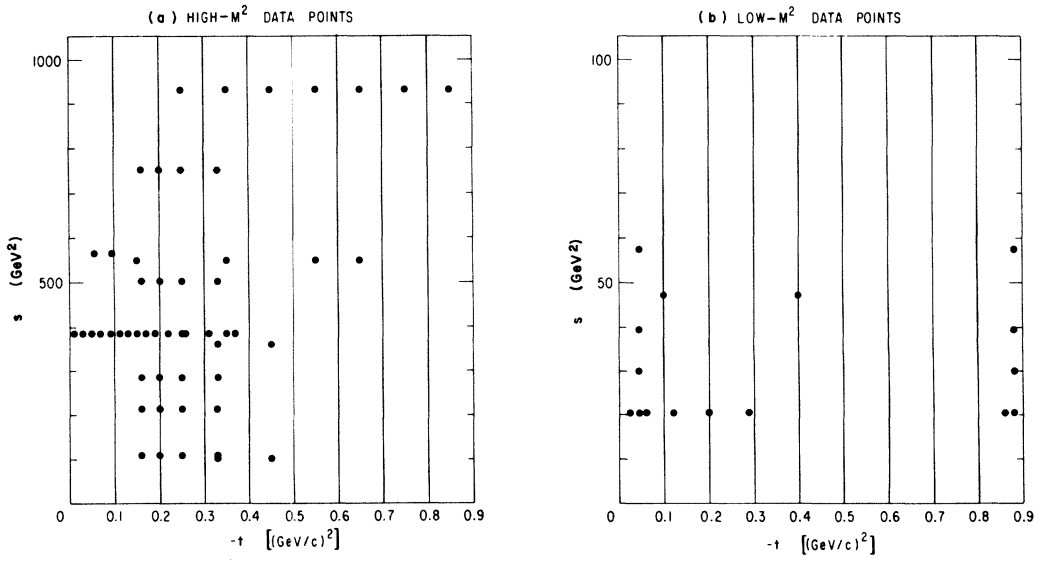

FIG. 4. Data points of $pp\to pX$ cross sections (Table I) plotted in an s-t plane.

TR couplings in the T_2 region are strongly affected by the T_1-region data. We may say, FF's TR couplings (especially the relative size of G_{ijP} and G_{ijR}) in the T_2 region are something like the "extrapolation" from those in the T_1 region. On the other hand, in the RR case the TR couplings are fitted at each fixed t, so the TR couplings in the T_2 region are determined only by the T_2-region data, which have very small density and which cover a very narrow s range, completely independently of the T_1-region data. Hence there arises such a large disagreement between RR and FF in the T_2 region, especially in the relative size of G_{PPP} and G_{PPR}.

This large disagreement shows that the estimation of TR couplings in the T_2 region obtained by using only existing data entails very large ambiguity. Here we note that both RR and FF input the FMSR data in the T_2 region in their χ^2 fits, so the FMSR is well satisfied in the T_2 region in their analyses [Fig. 9(b)].

B. Test of FMSR and duality

In the preceding we have estimated the TR parameters by using only *high*-M^2 data in order to calculate the rhs of Eqs. (2)–(8), i.e., Regge contributions. Now we estimate the lhs of Eqs. (2)–(8), i.e., resonance and background contributions, by integrating the *low*-M^2 spectra. Then we can test FMSR and duality by comparing the estimation of the rhs with that of the lhs. There are resonance-background separated low-mass data of Allaby *et al.*[19] and Edelstein *et al.*[20] in $0.1<|t|<0.5$ $(\mathrm{GeV}/c)^2$. They fitted the mass spectrum with the sum of Breit-Wigner forms and smooth polynomial background, e.g.,

$$\frac{d\sigma}{dtdM}=\sum_k C_k M^k+\sum_i \frac{a_i}{2\pi}\left[\frac{\Gamma_i}{(M-M_i)^2+(\Gamma_i/2)^2}\right], \tag{12}$$

where C_k is the coefficient of the polynomial, M_i and Γ_i are the mass and width of the ith resonance, and a_i represents the differential cross section of the ith resonance production, i.e., the area of Breit-Wigner curve. C_k, M_i, Γ_i, and a_i are the parameters of the χ^2 fit. In Table III is shown the value of each term of Eqs. (2)–(8) obtained this way at $P_{\mathrm{lab}}=24$ GeV/c, $t=-0.3$ $(\mathrm{GeV}/c)^2$, and $\bar{\nu}=3.0$ GeV^2.[28] In Fig. 5 are shown the semilocal versions of Eqs. (3)–(8) at $P_{\mathrm{lab}}=24$ GeV/c and $t=-0.4$ $(\mathrm{GeV}/c)^2$. In Fig. 6 the rhs and lhs of Eqs. (2)–(8) estimated this way are shown against s at $\bar{\nu}=3.0$ GeV^2 and $t=-0.2$, -0.3, and -0.4 $(\mathrm{GeV}/c)^2$.

From these we can say the data favor our normal scheme.[29] We see also that the FMSR Eq. (2) is well satisfied in the normal case. It is to be noted

TABLE III. The estimated value (in mb unit) of each term of Eqs. (2)–(8) at $p_{\mathrm{lab}}=24$ GeV/c, $t=-0.3$ $(\mathrm{GeV}/c)^2$, and $\bar{\nu}=3.0$ GeV^2. The low-mass data are taken from Ref. 19.

Low-mass data		Normal		Extreme		Abnormal I		Abnormal II	
I(Background)	0.504 ± 0.101	$PPP+RRP$	0.495 ± 0.066	$PPR+RRP$	1.009 ± 0.329	RRP	0.032 ± 0.004	RRP	0.032 ± 0.003
I(res)	0.927 ± 0.161	$PPR+RRR$	1.007 ± 0.346	$PPP+RRR$	0.492 ± 0.083	$PPP+\{PR\}R+RRR$	0.947 ± 0.212	$PPP+\{PR\}R+PPX$	5.050 ± 4.099
Total	1.431 ± 0.262	Total	1.502 ± 0.412	Total	1.502 ± 0.412	Total	0.979 ± 0.216	Total	5.081 ± 4.102
		PPP	0.464 ± 0.061			PPP	0.584 ± 0.054	PPP	0.572 ± 0.033
		RRP	0.030 ± 0.005			RRP	0.032 ± 0.004	RRP	0.032 ± 0.003
		PPR	0.979 ± 0.324			$\{PR\}R$	0.377 ± 0.123	$\{PR\}R$	0.237 ± 0.082
		RRR	0.028 ± 0.022			RRR	-0.014 ± 0.035	PPX	4.241 ± 3.984

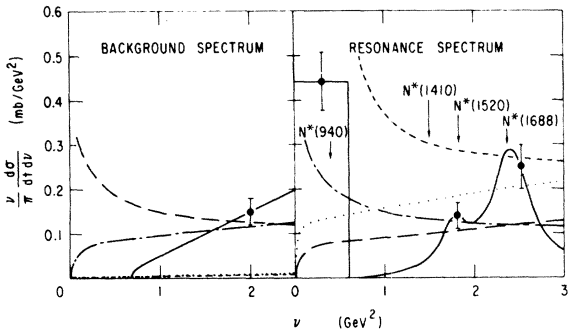

FIG. 5. Background and resonance spectra of $pp \to pX$ with typical error bars at $p_{lab} = 24$ GeV/c and $t = -0.4$ (GeV/c)^2 (Ref. 19). Dashed-dotted, long-dashed, dotted, and short-dashed curves represent the semilocal contribution of Regge exchange in normal, extreme, abnormal-I, and abnormal-II cases, respectively.

that the original abnormal scheme as well as our normal scheme can describe the resonances but that it gives too little background as seen in Fig. 5. There is a possibility that the inclusion of the neglected terms such as $\{PR\}P$ and PPR in the practical calculation may change this situation in the original abnormal scheme. However, even if such terms exist, they should be very small in the duality rules of Einhorn *et al.*[2]

Before closing this section we summarize our results as follows. The original abnormal duality scheme of Ref. 2 and the extreme abnormal duality scheme of Ref. 5 are inconsistent with the high-M^2 and resonance-background–separated low-M^2 data at least in $0.1 \lesssim |t| \lesssim 0.5$ (GeV/c)^2, while our normal scheme is quite consistent with the data in the same t region. The original abnormal

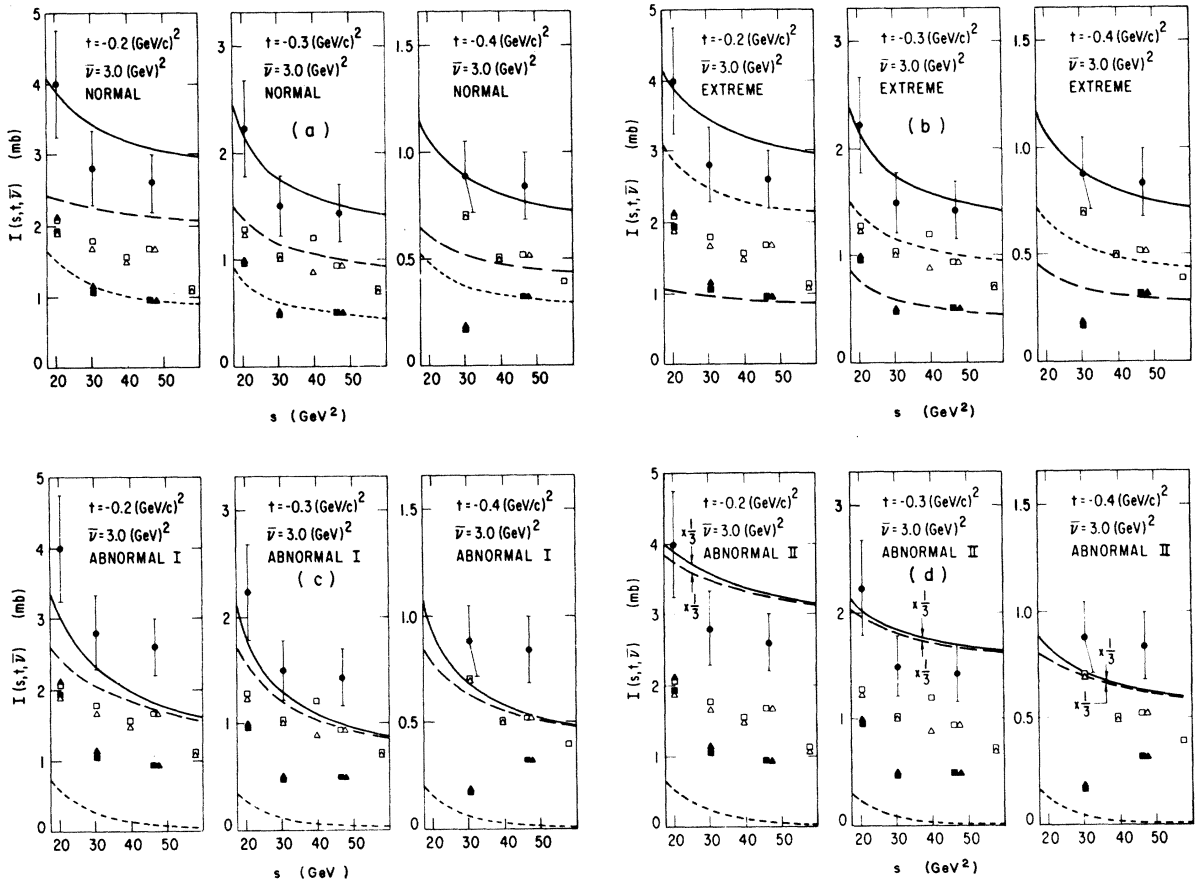

FIG. 6. Energy dependence of first-moment FMSR $I(s,t,\bar{\nu})$ at $\bar{\nu} = 3.0$ GeV^2 and $t = -0.2$, -0.3, and -0.4 (GeV/c)^2 estimated from the $pp \to pX$ data of Refs. 19 and 20 (filled circles). The open squares and triangles are the $pp \to pN^*$ resonance contribution to the FMSR. The filled squares and triangles are the background FMSR. The squares (triangles) correspond to the FMSR with $N^*(1410)$ taken as resonance (background). The solid, the long-dashed, and the short-dashed curves are the predictions of the complete FMSR, resonance FMSR, and background FMSR, respectively, (a) in the normal scheme, (b) in the extreme scheme, (c) in the original abnormal scheme I, and (d) in the original abnormal scheme II.

scheme of Ref. 2 is ruled out by our analysis, so we do not discuss this scheme in the following.

IV. DUALITY TEST INCLUDING INTERFERENCE TERMS

The test in Sec. III is based on the assumption of the absence of interference terms. In this section we examine whether the inclusion of the interference terms causes a drastic change of our conclusions in Sec. III. We estimate the rhs of Eqs. (2), (3), (4), (7), and (8) by performing a TR fit with five terms: PPP, $\{PR\}P$, RRP, PPR, and $\{PR\}R$. We neglect the RRR term since it is very small both in the high-M^2 and low-M^2 regions, as seen in Sec. III. We perform a TR fit for various values of the ratio $R \equiv G_{\{PR\}R}(t)/G_{PPR}(t)$ fixed at each t [$t=-0.2$, -0.3, and -0.4 (GeV/c)^2]. The t-channel trajectories $\tilde{\alpha}_R(t)$ in the $R_t R_t P_0$ term and $\alpha_P(t)$ are allowed to vary for an optimum fit at each fixed R. For the t-channel trajectory $\alpha_R(t)$ in the interference terms $\{P_t R_t\}P_0$ and $\{P_t R_t\}R_0$ we take an ordinary meson trajectory $\alpha_R(t)=t+0.5$ as π exchange does not interfere with P exchange by parity conservation in the small-t region [i.e., $\{P_t\pi_t\}P_0=\{P_t\pi_t\}R_0=0$].[30] For the "$t$"-channel trajectories of $ip\to jp$ scattering we take $\alpha_P(0)=1$ and $\alpha_R(0)=0.5$. In this case the TR formula Eq. (1) becomes

$$\frac{s}{\pi}\frac{d\sigma}{dtd\nu}=G_{PPP}(t)(1-x)^{1-2\alpha_P(t)}+G_{\{PR\}P}(t)(1-x)^{1-\alpha_P(t)-\alpha_R(t)}+G_{RRP}(t)(1-x)^{1-2\alpha_R(t)}$$
$$+G_{PPR}(t)(1-x)^{1/2-2\alpha_P(t)}\left(\frac{\nu_0}{s}\right)^{1/2}+G_{\{PR\}R}(t)(1-x)^{1/2-\alpha_P(t)-\alpha_R(t)}\left(\frac{\nu_0}{s}\right)^{1/2}. \quad (13)$$

We make χ^2 fit with four parameters G_{PPP}, $G_{\{PR\}P}$, G_{RRP}, and G_{PPR} for each fixed R. Here the trajectories $\alpha_P(t)$ and $\tilde{\alpha}_R(t)$ are allowed to vary for an optimum fit. The restriction $R \gtrsim R_0$ [$R_0=-3.1$ for $t=-0.2$, $R_0=-3.6$ for $t=-0.3$, and $R_0=-4.3$ for $t=-0.4$ (GeV/c)^2] is obtained from the experimental fact that the nonscaling part of the invariant cross section is positive at least in $0.8\lesssim x\lesssim 1.0$ and $0.1\lesssim|t|\lesssim 0.5$ (GeV/c)^2. The same high-s, *high-M^2* data used in Sec. III are input (Table I).

For the lhs of Eqs. (2), (3), (4), (7), and (8) we take the same estimations as obtained in Sec. III. We examine duality for each fixed R. In Fig. 7 are plotted the ratios rhs/lhs of Eqs. (2), (3), (4), (7), and (8) estimated this way at $P_{\rm lab}=24$ GeV/c and (a) $t=-0.4$ (GeV/c)^2, $\bar{\nu}=3.52$ GeV^2, (b) $t=-0.3$ (GeV/c)^2, $\bar{\nu}=3.42$ GeV^2, and (c) $t=-0.2$ (GeV/c)^2, $\bar{\nu}=3.32$ GeV^2 against $R'\equiv R/(1+|R|)$. The error of the estimation of the lhs of these equations is ~20%. The error of the estimation of the rhs is ~30% for Eq. (2), ~50% for Eq. (3), ~33% for Eq. (7), ~18% for Eq. (4), and ~30% for Eq. (8). When the ratio of rhs/lhs is close to one, then the scheme is good. From these we see that our normal scheme is consistent with the data for any R' value where FMSR Eq. (2) is well satisfied, while the extreme scheme is consistent with the data only for $0.65\lesssim R'\lesssim 0.85$ at $t=-0.2$ (GeV/c)^2, $0.5\lesssim R'\lesssim 0.85$ at $t=-0.3$ (GeV/c)^2, and $-0.50\lesssim R'\lesssim 0.75$ at $t=-0.4$ (GeV/c)^2. However, as is seen from the semilocal version of Eqs. (3), (4), (7), and (8) in Fig. 8, the extreme scheme is inconsistent even for the R' value [$0.65\lesssim R'\lesssim 0.85$ at $t=-0.2$ (GeV/c)^2,

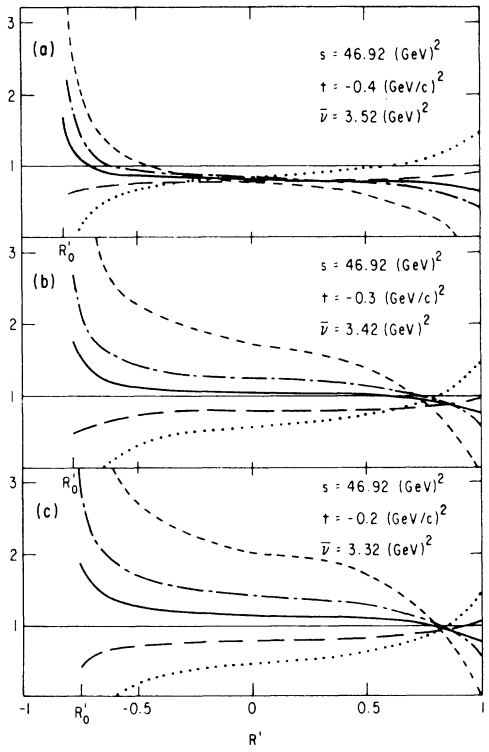

FIG. 7. The ratios of rhs to lhs of Eqs. (2), (3), (4), (7), and (8) at $p_{\rm lab}=24$ GeV/c and (a) $t=-0.4$ (GeV/c)^2, $\bar{\nu}=3.52$ GeV^2, (b) $t=-0.3$ (GeV/c)^2, $\bar{\nu}=3.42$ GeV^2, and (c) $t=-0.2$ (GeV/c)^2, $\bar{\nu}=3.32$ GeV^2 plotted against R'. The solid, long-dashed, dashed-dotted, short-dashed, and dotted curves correspond to Eqs. (2), (3), (4), (7), and (8), respectively. Here $R'_0\equiv R_0/(1+|R_0|)$. Low-mass data are taken from Ref. 19.

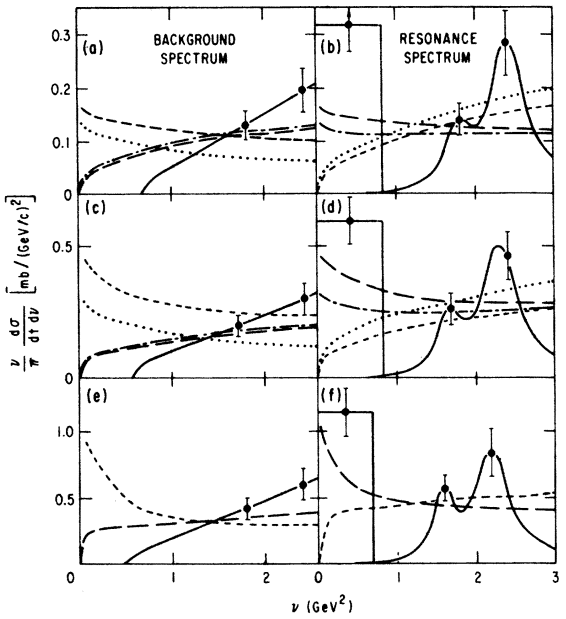

FIG. 8. Background and resonance spectra of $pp \to pX$ of Ref. 19 with typical error bars at p_{lab} 24 GeV/c and $t=-0.2$, -0.3, and -0.4 (GeV/c)^2. (a) and (b) The long-dashed and the short-dashed curves are the semilocal predictions at $t=-0.4$ (GeV/c)^2 of the normal and the extreme schemes for $R'=-0.2$, respectively. The dashed-dotted and the dotted curves are of the normal and the extreme schemes for $R'=0.5$, respectively. (c) and (d) The long-dashed and the short-dashed curves are the semilocal predictions at $t=-0.3$ (GeV/c)^2 of the normal and the extreme schemes for $R'=0.5$, respectively. The dash-dotted and dotted curves are of the normal and the extreme schemes for $R'=0.8$, respectively. (e) and (f) The long-dashed and the short-dashed curves are the semilocal predictions at $t=-0.2$ (GeV/c)^2 of the normal and the extreme schemes for $R'=0.8$, respectively.

$0.5 \lesssim R' \lesssim 0.85$ at $t=-0.3$ (GeV/c)^2, and $-0.5 \lesssim R' \lesssim 0.75$ at $t=-0.4$ (GeV/c)^2] where it seems to be consistent with the data in the global form. So we again obtain the result that the data favor our normal scheme. Hence we can say that inclusion of interference terms does not change our conclusions obtained in Sec. III.

V. RELIABILITY OF TEST (COMPARISON WITH OTHER DUALITY ANALYSIS)

In this section we discuss the reliability of our duality test comparing with the other duality analysis.[5] The duality test is beset with two uncertainties, i.e., P(scaling)-R(nonscaling) separation ambiguity and resonance-background separation ambiguity.

A. Reliability of our test (Sec. III and Sec. IV)

1. P-R separation. As is explained in Sec. III, the data have a very large density and *cover a very wide energy s range* in $0.1<|t|<0.5$ (GeV/c)^2 where we make TR fits, so we can say our P-R separation ambiguity is small.[31]

2. Resonance-background separation. Resonance-background separation ambiguity comes mainly from whether the $N^*(1410)$ peak is taken

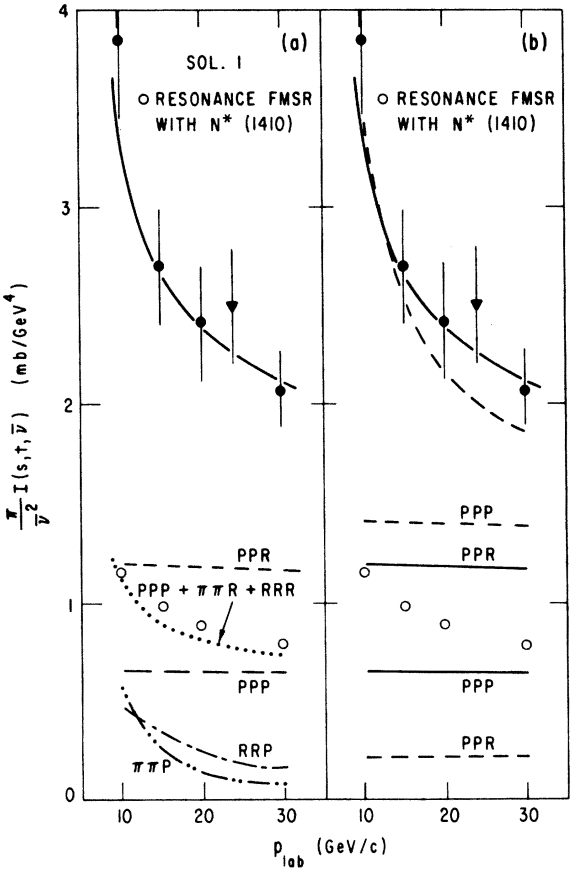

FIG. 9. (a) The energy dependence of the first-moment FMSR $(\pi/\bar{\nu}^2)I(s,t,\bar{\nu})$ at $t=-0.044$ (GeV/c)^2 and $\bar{\nu}=3.16$ GeV^2 constructed from the $pp \to pX$ data of Ref. 19 (filled circles) and Ref. 20 (filled triangle) compared with the results (solid line) of solution 1 of the TR analysis of FF (Fig. 17 of Ref. 5). The contribution to the FMSR of the each TR term is shown explicitly. The open circles represent the resonance contributions to the FMSR with $N^*(1410)$ taken as resonance. (b) The energy dependence of the first-moment FMSR $(\pi/\bar{\nu}^2)I(s, t,\bar{\nu})$ at $t=-0.044$ (GeV/c)^2 and $\bar{\nu}=3.16$ GeV^2 constructed from the $pp \to pX$ data of Refs. 19 and 20. The solid and dashed curves show the results of the TR analyses of FF (Ref. 5) (solution 1) and RR (Ref. 24) (Fig. 3 of Ref. 32). *PPP* and *PPR* contributions are shown explicitly. The open circles are the resonance contributions to the FMSR with $N^*(1410)$ taken as resonance.

as a pure resonance or not. However, the production cross section of the $N^*(1410)$ peak is nearly zero in $10 \lesssim P_{\text{lab}} \lesssim 30$ GeV/c and $0.2 \lesssim |t| \lesssim 0.4$ (GeV/c)^2 where we make duality analysis.[19,20]

B. Comparison with the test of FF[5]

FF[5] made a similar duality test to ours nearly at the same time as we.[6] They made TR fits with six terms PPP, PPR, RRP, RRR, $\pi\pi P$, and $\pi\pi R$ as is explained in Sec. III A 4 (II), and they tested duality at $t = -0.044$ and -0.88 (GeV/c)^2 in the same way as we. Their conclusion is contrary to ours. That is, both the diffractive components of resonances and background are dual to some combination of PPP and PPR with nonvanishing PPR (mixed duality). In their fits PPP and PPR are primarily dual to the diffractive resonance and background production, respectively, (extreme duality) and the normal duality is ruled out. One of their results is shown in Fig. 9(a).

We examine duality in $0.1 < |t| < 0.5$ (GeV/c)^2 (T_1 region) while FF examine it in $|t| < 0.1$ or $|t| > 0.5$ (GeV/c)^2 (T_2 region) [especially at $t = -0.044$ and -0.88 (GeV/c)^2]. As is explained in Sec. III A 4, the estimation of TR parameters [especially P(scaling)-R(nonscaling) separation] in the T_2 region obtained by using only existing data is accompanied by very large ambiguity in contrast to that in the T_1 region. Hoyer[32] also pointed out this fact. In Fig. 9(b) (Fig. 3 of Ref. 32) is shown the contribution to FMSR integral at $t = -0.044$ (GeV/c)^2 of each TR term in the TR fits of RR[24] and FF.[5] Their two analyses disagree with each other markedly, especially in the P(scaling)-R(nonscaling) separation.[33] In this respect we believe that the results of our duality test are more reliable than those of FF's test.

VI. CONCLUSION

We summarize our conclusion as follows. The original abnormal duality scheme in the framework of Ref. 2 and the extremely abnormal scheme of Ref. 5 are disfavored by our analysis at least in $0.1 \lesssim |t| \lesssim 0.5$ (GeV/c)^2. On the other hand our normal scheme is quite consistent with all the diffractive data of $pp \to pX$, $\pi^- p \to pX$, and $K^- p \to pX$ in the same t region.[7,8] We cannot say anything about the duality structure of diffraction dissociation in $|t| < 0.1$ or $|t| > 0.5$ (GeV/c)^2 for lack of data in these t regions.

After the computations reported in this article were completed, new sets of data[34,35,36] have become available. The ISR data in Ref. 34 and the Fermilab data in Ref. 35 are well reproduced in both normalization and shape with our TR parameters of the normal and extreme case fit. The Fermilab data of Ref. 36 at small M^2 values are also well described semilocally.

ACKNOWLEDGMENT

The author would like to express his gratitude to Professor E. L. Berger for reading this manuscript.

APPENDIX (DUALITY SCHEMES)

In the two-body case, the H-F duality scheme states as follows. The total cross section, which is equal to the imaginary part of the forward elastic amplitude by the optical theorem, has two components represented by the dual diagrams of Fig. 10. For Fig. 10(a), for the process $ab \to ab$, one has one pair of quark-antiquark lines going across, indicating resonance in the direct channel. The pair of quark-antiquark lines linking $a\bar{a}$ to $b\bar{b}$ means that for the process $ab \to ab$ one has meson trajectories being exchanged. The diagram 10(a) therefore represents the component in which direct-channel resonances are dual to meson exchange. In contrast, diagram 10(b) has 2 quark and 2 antiquark lines in the direct channel and none in the crossed channel; it represents then the component in which the background is dual to the exchange of the Pomeron.

We now apply the same language to inclusive cross sections, say for the reaction $ab \to aX$ in the fragmentation region of a.

(I) Our normal scheme. We propose a normal scheme which states as follows. The inclusive cross section of the process $ab \to aX(a \overset{b}{-} a)$, which is equal to the discontinuity of the forward three-body amplitude by Mueller's optical theorem, has six components in the limit of large s/M^2, where the exchanges in the $a\bar{a}$ channel Reggeize. Some of these six components are shown in Fig. 11. Interpreting these diagrams as before, one sees that for diagram 11(a) in both the direct channel $\bar{a}ab \to \bar{a}ab$ and the crossed channel $b\bar{b} \to a\bar{a}\,\bar{a}a$, one has one pair of quark-antiquark lines going across. Diagram 11(a) thus represents a component in which, as usual, direct-channel (i.e., the missing-mass channel) resonances are dual to the meson-

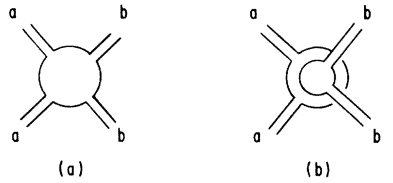

FIG. 10. The two duality components for the imaginary part of the forward elastic amplitude.

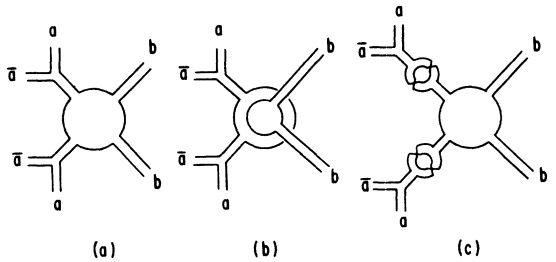

FIG. 11. Some duality components for the forward absorptive amplitude $\bar{a}ab \to \bar{a}ab$ in our normal scheme.

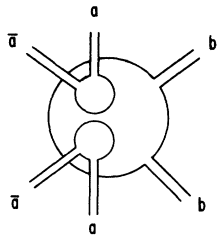

FIG. 12. A duality component for the forward absorptive amplitude $\bar{a}ab \to \bar{a}ab$ in the original abnormal scheme.

exchange term of the inclusive cross section. Diagram 11(a) contains ordinary Reggeon-particle scattering, since in the $a\bar{a}$ channel one has a pair of quark-antiquark lines going across. So diagram 11(a) represents the RRR term dual to the nondiffractively produced resonances. Similarly, the diagram 11(b) would represent a component which has the Pomeron exchange dual to a background, i.e., the RRP term dual to the nondiffractive background. As for the diagram 11(c), in the $a\bar{a}$ channel one has no quark line going across, so the diagram 11(c) contains *Pomeron-particle scattering*. Diagram 11(c) would represent a component which has *the meson exchange dual to resonances*, i.e., the PPR term dual to the diffractive resonances. Similar statements can be made for the other three components and finally Eqs. (3) and (4) are obtained in our normal scheme.

(II) Original abnormal scheme of Ref. 2. Einhorn *et al.* proposed an abnormal scheme which states as follows. The inclusive cross section of the process $ab \to aX\,(a \overset{b}{-} a)$ has five components. One of these components shown in Fig. 12 has a singular dual structure. One see that, in the direct (missing-mass) channel, one has a pair of quark-antiquark lines, indicating resonances. Whereas, in the crossed channel, one has no quark line implying therefore Pomeron exchange. This diagram contains *Pomeron-particle scattering*, since in the $a\bar{a}$ channel one has no quark line going across. This diagram would thus represent a component which has *a Pomeron dual to direct-channel resonances*, i.e., the PPP term dual to the diffractive resonances. Hence it is called abnormal dual component. The similar statement can be made for the other components and finally Eqs. (5) and (6) are obtained in the original abnormal scheme. Notice that in this scheme there is no natural place for the triple-Regge terms PPR, PRP, and RPP, so these terms should vanish or be very small.

---

*Work performed under the auspices of the United States Energy Research and Development Administration.

[1]P. Hoyer, R. G. Roberts, and D. P. Roy, Nucl. Phys. B56, 173 (1973).
[2]M. B. Einhorn, M. B. Green, and M. A. Virasoro, Phys. Lett. 37B, 292 (1971); Phys. Rev. D 7, 102 (1973).
[3]Chang Hong-Mo, H. I. Miettinen, and R. G. Roberts, Nucl. Phys. B54, 411 (1973).
[4]R. G. Roberts and D. P. Roy, Phys. Lett. 47B, 247 (1973).
[5]R. D. Field and G. C. Fox, Nucl. Phys. B80, 367 (1974).
[6]K. Hidaka, Lett. Nuovo Cimento 11, 503 (1974).
[7]K. Hidaka, Lett. Nuovo Cimento 12, 273 (1975).
[8]K. Hidaka, Lett. Nuovo Cimento 15, 221 (1976).
[9]K. Abe *et al.*, Phys.Rev. Lett. 31, 1527 (1973).
[10]M. G. Albrow *et al.*, Nucl. Phys. B72, 376 (1974).
[11]M. G. Albrow *et al.*, Nucl. Phys. B54, 6 (1973).
[12]S. J. Barish *et al.*, Phys. Rev. Lett. 31, 1080 (1973).
[13]J. Whitmore *et al.*, Phys. Rev. D 11, 3124 (1975).
[14]J. W. Chapman *et al.*, UR Report No. UR458 (UHBC 73-21) (unpublished).
[15]F. Sannes *et al.*, Phys. Rev. Lett. 30, 766 (1973).
[16]J. Kwiecinski, Lett. Nuovo Cimento 3, 619 (1972); M. B. Einhorn, J. Ellis, and J. Finkelstein, Phys. Rev. D 5, 2063 (1972).
[17]FF did not refer to the duality of $\{PR\}P$ and $\{PR\}R$ terms in Ref. 5. There is no dual-diagram theory that gives these terms an abnormal duality assignment, i.e., $\{PR\}P$ contributing to resonances and $\{PR\}R$ contributing to background. So we take a normal duality assignment for them here. In any case, as is seen in the practical calculation done in Sec. IV, they are not so large that our conclusions on the duality test depend on the duality assignment for them.
[18]F. E. Paige and L.-L. Wang, Nucl. Phys. B46, 477 (1972).
[19]J. V. Allaby *et al.*, Nucl. Phys. B52, 316 (1973).
[20]R. M. Edelstein *et al.*, Phys. Rev. D 5, 1073 (1972).
[21]S. Childress *et al.*, Phys. Rev. Lett. 32, 389 (1974).
[22]M. G. Albrow *et al.*, Nucl. Phys. B51, 388 (1973).
[23]Bonn-Hamburg-Munchen collaboration, paper submitted to Aix-en-Provence Conference, 1973 (unpublished).

[24]M. Bishari, Phys. Lett. 38B, 510 (1972); K. Abe *et al.*, Phys. Rev. Lett. 31, 1530 (1973); R. G. Roberts and D. P. Roy, Nucl. Phys., B77, 240 (1974).
[25]We take the statistical errors, which are large in general, plus the systematic errors as the errors of the input data for the TR fit. Hence the small χ^2 values arise.
[26]F. T. Dao *et al.*, Phys. Lett. B45, 399 (1973); F. T. Dao *et al.*, Phys. Lett. B45, 402 (1973).
[27]Here it is to be noted that the relative size of G_{ijP} (coupling of scaling term) and G_{ijR} (coupling of non-scaling term) is mainly determined by the *s dependence* of the data.
[28]Each term of rhs of Eqs. (3)–(8) depends on $\alpha'_P(0)$ and $\alpha_R(0)$ so slightly that our conclusion of duality test does not change with the way of the choice of the values of $\alpha'_P(0)$ and $\alpha_R(0)$.
[29]It is possible that the background, which is obtained by fitting the mass spectrum by a sum of Breit-Wigner forms and a polynomial term (Refs. 19,20) is over-estimated as it may contain weak secondary resonances such as daughters.
[30]R. D. Field, Caltech Report No. CALT-68-459, 1974 (unpublished).
[31]See Ref. 27.
[32]P. Hoyer, in *Proceedings of the XVII International Conference on High Energy Physics, London*, 1974, edited by J. R. Smith (Rutherford Laboratory, Chilton, Didcot, Berkshire, England, 1974), p. I-158.
[33]As is explained in Sec. III A (4) they both input the FMSR data (besides high-M^2 data) in this T_2 region in the χ^2 fit, so FMSR is well satisfied at $t=-0.044$ $(\mathrm{GeV}/c)^2$ (T_2 region) in these two analyses.
[34]M. G. Albrow *et al.*, Nucl. Phys. B108, 1 (1976).
[35]R. L. Anderson *et al.*, Phys. Rev. Lett. 38, 880 (1977).
[36]R. L. Anderson *et al.*, Phys. Rev. Lett. 37, 1724 (1976).